DISCRETE AND CONTINUOUS
DYNAMICAL SYSTEMS SERIES S
Volume **6**, Number **2**, April **2013**

doi:10.3934/dcdss.2013.6.293

pp. **293–316**

FREE ENERGIES AND PSEUDO-ELASTIC TRANSITIONS FOR SHAPE MEMORY ALLOYS

Alessia Berti

Facoltà di Ingegneria, Università e-Campus
22060 Novedrate (CO), Italy

Claudio Giorgi and Elena Vuk

Dipartimento di Matematica, Università di Brescia
25133 Brescia, Italy

Abstract. A one-dimensional model for a shape memory alloy is proposed. It provides a simplified description of the pseudo-elastic regime, where stress-induced transitions from austenitic to oriented martensitic phases occurs. The stress-strain evolution is ruled by a bilinear rate-independent o.d.e. which also accounts for the fine structure of minor hysteresis loops and applies to the case of single crystals only. The temperature enters the model as a parameter through the yield limit y. Above the critical temperature $\theta^*_{\mathcal{A}}$, the austenite-martensite phase transformations are described by a Ginzburg-Landau theory involving an order parameter φ, which is related to the anelastic deformation. As usual, the basic ingredient is the Gibbs free energy, ζ, which is a function of the order parameter, the stress and the temperature. Unlike other approaches, the expression of this thermodynamic potential is derived rather then assumed, here. The explicit expressions of the minimum and maximum free energies are obtained by exploiting the Clausius-Duhem inequality, which ensures the compatibility with thermodynamics, and the complete controllability of the system. This allows us to highlight the role of the Ginzburg-Landau equation when phase transitions in materials with hysteresis are involved.

1. **Introduction.** From a macroscopic point of view, austenite ($\mathcal{A}$) is a solid phase, usually characterized by a body centered cubic crystallographic structure, which transforms into martensite by means of a lattice shearing mechanism. The martensite phase can exist in two states: self-accommodated, or "twinned", martensite ($\mathcal{M}_t$) and oriented, or "detwinned", martensite ($\mathcal{M}_d$). The twinned martensite is formed by simple cooling under no external loading; then, variants of equal volume fractions form in a self-accommodated fashion and no signicant macroscopic strain is incurred. In contrast, oriented martensite is produced by an applied stress and, consequently, the martensitic variants are preferably oriented by the direction of the external force. This oriented martensite induces a macroscopic strain and can be formed either from phase transformation of austenite under a mechanical loading or from reorientation of self-accommodated martensite. Under one-dimensional tensile processes, the oriented martensite ($\mathcal{M}_d$) occurs with opposite orientation, $\mathcal{M}^-$ and

2010 *Mathematics Subject Classification.* Primary: 74N30; Secondary: 74C05, 74F05, 80A22.

Key words and phrases. Shape memory alloys, austenite-martensite transition, pseudo-elasticity, hysteresis loops, stress-rate materials, free energy potentials, Ginzburg-Landau theory.

This work was produced under the auspices of GNFM–INDAM.

$\mathcal{M}^+$. Accordingly, the twinned martensite ($\mathcal{M}_t$) will be denoted by $\mathcal{M}^\pm$ (see, for instance, [1, 5]).

The thermomechanical phase transformation produces two unique effects: the shape memory effect and pseudo-elasticity (see, for instance, [7, 8]). The *shape memory effect* consists in the chance that a large permanent strain upon unloading may be recovered by heating the sample, whereas *pseudo-elasticity* results in a large non-linear inelastic strain recoverable upon unloading. As the temperature grows, both upper and lower loops move upward and downward, respectively, without significantly changing their shape (see Fig.1).

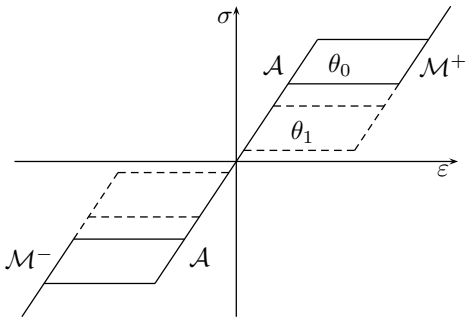

FIGURE 1. The dependence of the major hysteresis loop on the temperature in the pseudo-elastic regime: $\theta_0 > \theta_1$.

In the one-dimensional pseudo-elastic regime, a mix of just two phases occurs: $\mathcal{A}$ and $\mathcal{M}^+$, in tension, $\mathcal{A}$ and $\mathcal{M}^-$, in compression. Usually, transitions between them are described by an order parameter φ such that $\varphi = 0$ in $\mathcal{A}$, $\varphi = 1$ in $\mathcal{M}^+$, $\varphi = -1$ in $\mathcal{M}^-$. On the other hand, at lower temperature the material behavior is completely different. It resembles the behavior of an elastic-plastic body and involves three phases: $\mathcal{M}^+$, $\mathcal{M}^-$ and $\mathcal{M}^\pm$. The analysis of this regime, called pseudo-plastic, is outside the aim of this paper.

In this paper we confine our attention to the pseudo-elastic regime of a shape memory alloy and to the austenite-martensite phase transformations occurring therein. In Sect. 2 we provide a simplified description of the pseudo-elastic regime at a given temperature θ above the critical temperature $\theta^*_{\mathcal{A}}$. In Sect. 3 the stress-strain evolution is ruled by a bilinear rate-independent o.d.e. which also accounts for the fine structure of minor hysteresis loops and applies to the case of single crystals only. Stress-induced transformations $\mathcal{A} \leftrightarrow \mathcal{M}^+$ involve the yield limit y, which linearly depends on temperature. The complete controllability of the resulting dynamical system is provided in Sect. 4 by proving that each stress-strain state is accessible from and controllable at the origin. The point, here, is to estimate the amount of work expended or absorbed during suitable control processes in order to minimize the former and maximize the latter. Sect. 5 is devoted to exhibit the explicit forms of the minimum and maximum free energies. The former represents the maximum amount of work which may be extracted from the system when moving from a generic state to the origin. The latter represents the minimum amount of work which is required to supply to the system when attaining a generic state from the origin. Their expressions are obtained by exploiting the Clausius-Duhem inequality, which ensures the compatibility with thermodynamics. In Sect. 6

we exploit the minimum (Gibbs) free energy representation in the framework of a Ginzburg-Landau theory involving an order parameter φ, which is related to the anelastic deformation. This allows us to highlight the role of the Ginzburg-Landau equation when phase transitions in materials with hysteresis are involved. Finally, we compare our model with others recently appeared in the literature [3, 4, 9, 12].

2. **The pseudo-elastic regime.** At high temperature, a shape memory alloy (SMA) at rest is in the austenitic phase. When it is stressed, the material changes its lattice structure from a high-symmetry phase (austenite) to a lower-symmetry phase (martensite). This phenomenon is a stress-induced transition, which gives rise to a hysteresis loop.

At a given positive applied stress $\sigma_0 > 0$, forward ($\mathcal{A} \to \mathcal{M}^+$) and reverse ($\mathcal{M}^+ \to \mathcal{A}$) transformations are delimited by four characteristic temperatures $\mathcal{M}_f$, $\mathcal{M}_s$, $\mathcal{A}_s$ and $\mathcal{A}_f$, where the subscripts $_f$ and $_s$ mean *final* and *starting*, respectively (see Fig.2 a). For most alloys, they are related such that $\mathcal{M}_f < \mathcal{M}_s < \mathcal{A}_s < \mathcal{A}_f$, but for some materials the differences $\mathcal{M}_f - \mathcal{M}_s$ and $\mathcal{A}_f - \mathcal{A}_s$ are so small that forward and reverse transitions are characterized by two temperatures only, namely $\theta_{\mathcal{M}} = \mathcal{M}_f \approx \mathcal{M}_s$ and $\theta_{\mathcal{A}} = \mathcal{A}_f \approx \mathcal{A}_s$.

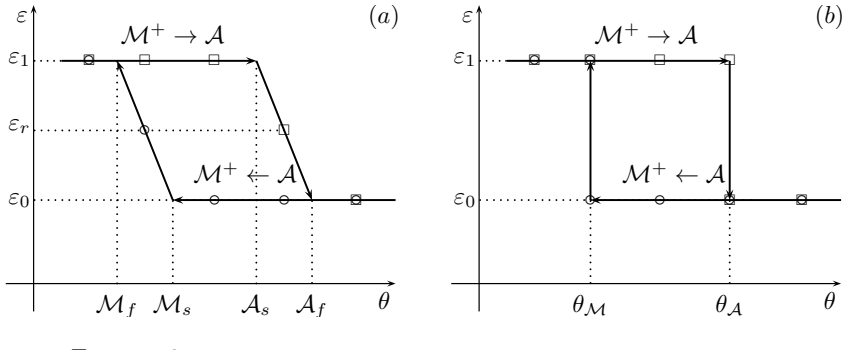

FIGURE 2. The strain-temperature hysteresis loop at $\sigma = \sigma_0 > 0$: (a) linear hardening, (b) no hardening.

The forward $\mathcal{A} \to \mathcal{M}^+$ transformation is obtained by decreasing temperature and is represented by the lower path in Fig. 2 a - 2 b (see also Fig. 3 and 4 following small circles from the left to the right). On the contrary, by increasing the temperature, the upper path in Fig. 2 a - 2 b is achieved. It represents the reverse transformation $\mathcal{M}^+ \to \mathcal{A}$ (see also Fig. 3 and 4 following small squares from the right to the left). Of course, all the transition temperatures so introduced depend on the reference stress σ_0 and their values increase as the stress grows and decrease as $\sigma_0 \to 0$.

In view of the modeling procedure developed in this paper, the description of the general case (and four transition temperatures) can be easily obtained from a basic model with no hardening (see, for instance, § 3). So, hereafter we assume that both $\mathcal{A} \to \mathcal{M}^+$ and $\mathcal{M}^+ \to \mathcal{A}$ transitions instantly occur at $\theta = \theta_{\mathcal{M}}$ and $\theta = \theta_{\mathcal{A}}$, respectively (see Fig. 2 b and 4).

When a transition temperature is reached, either $\theta_{\mathcal{A}}$ or $\theta_{\mathcal{M}}$, the stress σ_0 represents the corresponding *transformation stress*. Namely, its value gives either the *unloading critical stress*, $\sigma_{\mathcal{A}}$, when $\theta = \theta_{\mathcal{A}}$, or the *loading critical stress*, $\sigma_{\mathcal{M}}$, when

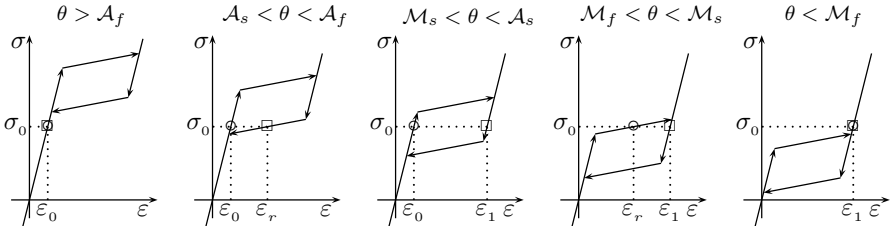

FIGURE 3. The $\mathcal{A} \to \mathcal{M}^+$ and $\mathcal{M}^+ \to \mathcal{A}$ temperature-induced transitions with linear hardening at $\sigma = \sigma_0 > 0$.

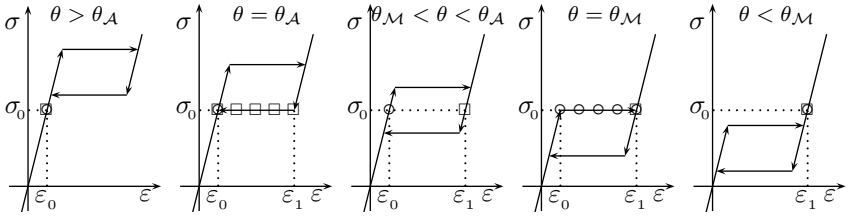

FIGURE 4. The $\mathcal{A} \to \mathcal{M}^+$ and $\mathcal{M}^+ \to \mathcal{A}$ temperature-induced transitions at $\sigma = \sigma_0 > 0$ (no hardening).

$\theta = \theta_{\mathcal{M}}$ (see Fig. 5 a). According to experimental findings, both transition temperatures decrease linearly as $\sigma_0 \to 0$ (see, for instance, [13]). In particular, $\theta_{\mathcal{A}}$ attains its minimum value when $\sigma_0 = 0$ and we let

$$\theta^*_{\mathcal{A}} = \theta_{\mathcal{A}}|_{\sigma_0=0} = \min_{\sigma_0 \geq 0} \theta_{\mathcal{A}}\,.$$

At $\theta = \theta^*_{\mathcal{A}}$, the *transformation stress* is denoted by σ_t and the residual deformation, which is named *transformation strain*, by ε_t (see Fig. 5 b).

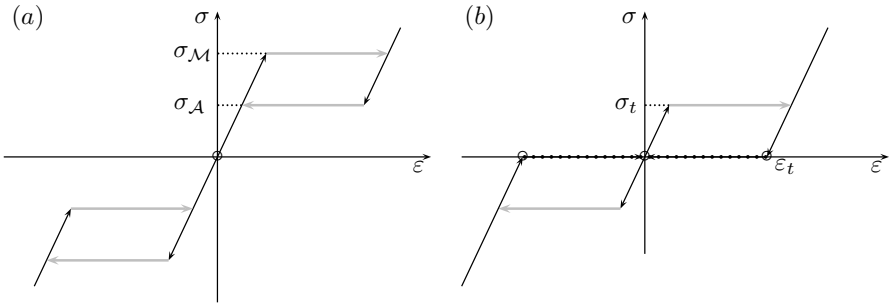

FIGURE 5. The $\mathcal{A} \to \mathcal{M}$ temperature-induced transitions at $\sigma_0 = 0$ and (a) $\theta = \theta_0 > \theta^*_{\mathcal{A}}$, (b) $\theta = \theta^*_{\mathcal{A}}$.

The hysteresis loop is also assumed to preserve its shape as the temperature changes, so that we have

$$\varepsilon_t = \varepsilon_1 - \varepsilon_0\,, \qquad \sigma_t = \sigma_{\mathcal{M}} - \sigma_{\mathcal{A}},$$

where ε_1 and ε_0 are given as in Fig. 4.

In order to describe the behavior of the system, a phase-transition diagram in the $(\theta, \sigma)-$plane is obtained in Fig. 6. The *pseudo-elastic* behavior is depicted by representing both critical (yield) stresses, $\sigma_{\mathcal{A}}$ and $\sigma_{\mathcal{M}}$, as linear functions of θ and assuming that their difference is independent of θ, $\sigma_{\mathcal{M}} - \sigma_{\mathcal{A}} = \sigma_t$.

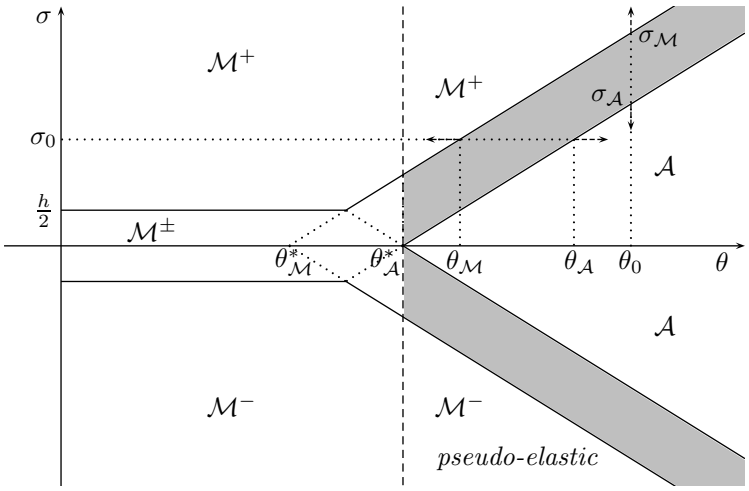

FIGURE 6. The (θ, σ)-diagram of the pseudo-elastic regime: arrows denote temperature- and stress-induced phase transitions.

Accordingly, in this range $\theta_{\mathcal{A}} - \theta_{\mathcal{M}} = \eta$ is a constant. In this framework, temperature-induced transitions move on horizontal lines (for instance, at $\sigma = \sigma_0$: cf. Fig. 4), whereas stress-induced transitions move on vertical lines (for instance, at $\theta = \theta_0$: cf. Fig. 5 a). Below $\theta^*_{\mathcal{A}}$ the pseudo-elastic regime is lost, since a residual strain ε_t remains after unloading (cf. Fig. 5 b).

This qualitative behavior can be modeled by assuming that $\sigma_{\mathcal{M}}$ depends on θ, namely $\sigma_{\mathcal{M}} = y(\theta)$ and $\sigma_t = h$ is a constant. At temperatures above $\theta^*_{\mathcal{A}}$, $y(\theta)$ linearly reduces as θ decreases until it reaches the constant value h at $\theta = \theta^*_{\mathcal{A}}$ (cf. Fig. 5). Finally, we let $\theta^*_{\mathcal{M}} = \theta^*_{\mathcal{A}} - \eta$ and

$$y(\theta) = \frac{h}{\eta}(\theta - \theta^*_{\mathcal{A}}) + h\,, \qquad \theta \geq \theta^*_{\mathcal{A}}\,. \tag{1}$$

3. **The stress-rate model.** In this section we restrict our attention to spatially homogeneous and isothermal one-dimensional processes. If this is the case, absolute temperature enters the constitutive relations of the model just as a positive parameter.

At temperatures above $\theta^*_{\mathcal{A}}$ and under mechanical loading, the material exhibits an elastic behavior until a critical stress σ_A is reached. At this stress level the material undergoes a stress-induced phase transformation $(A \to B)$ from austenite to martensite during which large inelastic strains are developed. When the point B is reached, upon unloading the reverse phase transformation (martensite-to-austenite) takes place during which an elastic deformation $(B \to D)$ and a non-linear deformation $(D \to C)$ follow. This phenomenon is called pseudo-elasticity: it is "elastic" in the sense that, in a loading-unloading process, the original state is completely recovered, but it is partially inelastic, since, in such an experiment, a hysteresis loop

occurs (see Fig. 7) and some amount of energy, which is proportional to the loop area, is dissipated.

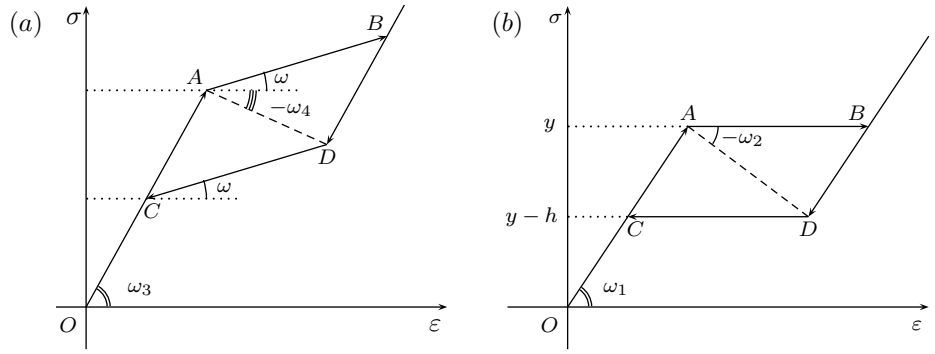

FIGURE 7. The major hysteresis loop inside the pseudo-elastic regime: (a) hardening occurs beyond the yield limit; (b) no hardening occurs.

In a uniaxial loading-unloading experiment without hardening (see Fig. 7 b), the shape of the major hysteresis loop looks like a parallelogram and is characterized by the following material parameters: the *(forward) transformation stress* or *yield limit*, $y = \sigma_{\mathcal{M}} > 0$, and the *yield gap*, $h = \sigma_{\mathcal{M}} - \sigma_{\mathcal{A}} = \sigma_t > 0$, jointly with the slopes of the *elastic line*, OA, and the *skeleton line*, AD, which are denoted by α and $-\kappa$ where

$$\tan\omega_1 = \alpha, \qquad \tan\omega_2 = \kappa.$$

Accordingly, this model is named *bilinear*. If some hardening occurs beyond the yield limit, a further parameter, β, is needed (see Fig. 7 a) where $\tan\omega = \beta$, $\tan\omega_3 = \alpha + \beta$ and $\tan\omega_4 = \kappa - \beta$. If this is the case, however, it is easy to check that the graph of the major loop and, what is more, the evolution equation describing the minor loops can be both obtained from the model without hardening by means of the linear transformation

$$\varepsilon \quad \to \quad \varepsilon, \tag{2}$$

$$\sigma \quad \to \quad \sigma + \beta\varepsilon. \tag{3}$$

Hereafter, we restrict our attention to the case when no hardening occurs.

Since the hysteresis loop does not significantly change its shape as the temperature varies in the pseudo-elastic regime, only the material parameter y is allowed to depend on θ, whereas h, α, κ (and β, eventually) keep a constant positive value for all temperatures above $\theta^*_{\mathcal{A}}$. By virtue of assumption (1), $y(\theta)$ is a linear increasing function and $y > h$ holds. Accordingly, the *reverse transformation stress*, $\sigma_{\mathcal{A}} = y(\theta) - h$, is positive for all $\theta > \theta^*_{\mathcal{A}}$ and during any loading-unloading experiment the strain ε goes back to the origin upon complete unloading.

At a given temperature $\theta > \theta^*_{\mathcal{A}}$, the major hysteresis loop looks like a parallelogram whose vertices A, B, C, D have the following coordinates in the (ε, σ)-plane:

$$\begin{aligned} A &= \left(\frac{y}{\alpha}, y\right), & B &= \left(\frac{y}{\alpha} + h\left[\frac{1}{\kappa} + \frac{1}{\alpha}\right], y\right), \\ C &= \left(\frac{y}{\alpha} - \frac{h}{\alpha}, y - h\right), & D &= \left(\frac{y}{\alpha} + \frac{h}{\kappa}, y - h\right). \end{aligned} \tag{4}$$

The length of AB and CD given by $\varepsilon_t = h(1/\kappa+1/\alpha)$ is constant and independent of the temperature, which is in agreement with experimental findings. The stress-strain pairs on the diagonal AD represent thermodynamically unstable equilibrium states (cf. [12]). In order to model major and minor hysteresis loops as in Fig. 8, we introduce the following rate-type stress-strain constitutive equation,

$$\dot\sigma = \mathcal{F}(\varepsilon, \sigma, \operatorname{sgn}\dot\varepsilon)\dot\varepsilon, \tag{5}$$

where the symbol sgn denotes the sign of a function, *i.e.*

$$\operatorname{sgn} P = \begin{cases} 1 & \text{if } P > 0, \\ 0 & \text{if } P = 0, \\ -1 & \text{if } P < 0. \end{cases}$$

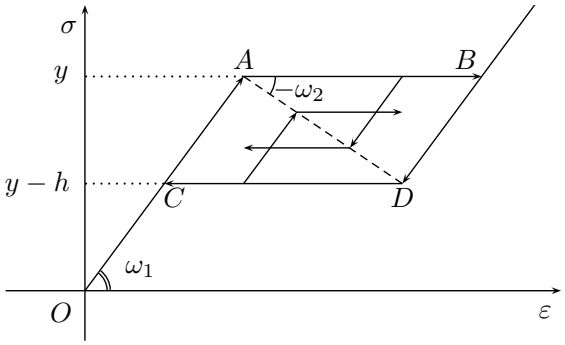

FIGURE 8. The bilinear model: major and minor loops ($\alpha = \tan\omega_1$, $\kappa = \tan\omega_2$).

In the region Ξ occupied by the major loop, the stress-strain rate $\mathcal{F}$ is defined as

$$\mathcal{F}(\varepsilon, \sigma, \operatorname{sgn}\dot\varepsilon) = \begin{cases} \alpha & \text{if} \quad (\varepsilon,\sigma) \in \mathcal{S}_1 \cup \mathcal{S}_2 \text{ or} \\ & \qquad (\varepsilon,\sigma) \in \mathcal{P}_2 \cup \Xi_1 \text{ and } \operatorname{sgn}\dot\varepsilon = 1 \text{ or} \\ & \qquad (\varepsilon,\sigma) \in \mathcal{P}_1 \cup \Xi_2 \text{ and } \operatorname{sgn}\dot\varepsilon = -1 \\ 0 & \text{otherwise,} \end{cases} \tag{6}$$

where the region $\Xi = \Xi_1 \cup \Xi_2 \cup \mathcal{S}$ is composed by two triangular domains (see Fig. 9)

$$\begin{aligned} \Xi_1 &= \{(\varepsilon,\sigma) \in \mathbb{R}^2 : y - h \le \sigma < y,\ \frac{\sigma}{\alpha} < \varepsilon < -\frac{\sigma}{\kappa} + \frac{\alpha+\kappa}{\alpha\kappa} y\}, \\ \Xi_2 &= \{(\varepsilon,\sigma) \in \mathbb{R}^2 : y - h < \sigma \le y,\ -\frac{\sigma}{\kappa} + \frac{\alpha+\kappa}{\alpha\kappa} y < \varepsilon < \frac{\sigma}{\alpha} + \frac{\alpha+\kappa}{\alpha\kappa} h\}, \end{aligned}$$

and a piecewise linear graph $\mathcal{S} = \mathcal{S}_* \cup \mathcal{S}_1 \cup \mathcal{S}_2 \cup \mathcal{P}_1 \cup \mathcal{P}_2$ (the *skeleton curve*) with

$$\begin{aligned} \mathcal{S}_* &= \left\{(\varepsilon,\sigma) \in \mathbb{R}^2 : \sigma = -\kappa\varepsilon + \frac{k+\alpha}{\alpha} y,\ \frac{y}{\alpha} < \varepsilon < \frac{y}{\alpha} + \frac{h}{\kappa}\right\} = AD, \\ \mathcal{S}_1 &= \left\{(\varepsilon,\sigma) \in \mathbb{R}^2 : \sigma = \alpha\varepsilon,\ 0 \le \varepsilon < \frac{y}{\alpha}\right\} = OA, \\ \mathcal{S}_2 &= \left\{(\varepsilon,\sigma) \in \mathbb{R}^2 : \sigma = \alpha\varepsilon - \frac{\alpha+\kappa}{\kappa} h,\ \varepsilon > \frac{y}{\alpha} + \frac{h}{\kappa}\right\} \supset DB, \\ \mathcal{P}_1 &= \left\{\left(\frac{y}{\alpha}, y\right)\right\} = A, \qquad \mathcal{P}_2 = \left\{\left(\frac{y}{\alpha} + \frac{h}{\kappa}, y - h\right)\right\} = D. \end{aligned}$$

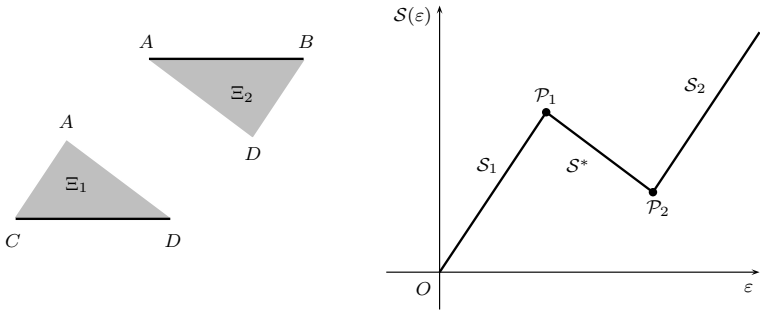

FIGURE 9. The region Ξ: on the left the triangular Ξ_1, Ξ_2, on the right the skeleton curve $\mathcal{S} = \mathcal{S}_* \cup \mathcal{S}_1 \cup \mathcal{S}_2 \cup \mathcal{P}_1 \cup \mathcal{P}_2$.

During the mechanical deformation of the sample, other memory effects than hysteresis can also occur at both the microscopic and macroscopic scale, for instance viscoelastic-relaxation and ageing. Henceforth we assume that pseudo-elastic hysteresis represents the main aspect of mechanical behavior of the sample, and we neglect any other memory phenomenon, consequently. Hysteresis is distinguished from other memory effects because it exhibits permanent memory. Furthermore, it satisfies the properties of rate-independence and piecewise monotonicity. Such characteristics are discussed in detail in [6, §12], for instance, and our assumptions are modeled accordingly.

4. **Complete controllability and mechanical work.** This section is devoted to establish the complete controllability of the dynamical system (5)-(6). To this end, we first introduce the concepts of (isothermal) process and state.

A *mechanical process* p is a map $p : [0, d_p) \to \mathbb{R}$, which is piecewise continuous on the time interval $[0, d_p)$, $d_p > 0$, and changes its sign at most a finite number of times. The quantity d_p denotes the finite duration of p. Henceforth, we identify the process with the rate of deformation, namely

$$p(t) = \dot{\varepsilon}(t), \qquad t \in [0, d_p).$$

Two processes, p_1 and p_2, with different durations, d_1 and d_2, respectively, can be composed into a single process $p = p_1 * p_2$ according to the following formula,

$$p(t) = p_1 * p_2(t) = \begin{cases} p_1(t) & t \in [0, d_1), \\ p_2(t - d_1) & t \in [d_1, d_1 + d_2). \end{cases} \tag{7}$$

By virtue of the rate-independence, we are allowed to restrict our attention to the set Π of all processes which are composed only by piecewise constant functions with value $+1$ or -1 (see, for instance, [6, §12]), namely

$$p(t) = \begin{cases} +1 & t \in I_i^+, \quad i = 1, ..., n \\ -1 & t \in I_j^-, \quad j = 1, ..., m, \end{cases} \tag{8}$$

where I_i^+ and I_j^- represent disjoint subintervals of $[0, d_p)$ whose union covers the whole interval. Hence, the graph of the deformation $\varepsilon(t)$ corresponding to any process $p \in \Pi$ is composed by straight lines with slope $+1$ or -1, but different length ($|I_i^+|$ and $|I_i^-|$, respectively).

The local *mechanical state* of the material is characterized by the pair

$$\xi(t) = (\varepsilon(t), \sigma(t)) \in \Xi.$$

Indeed, given any process $p \in \Pi$ and any initial state $\xi_0 = (\varepsilon_0, \sigma_0)$, one can determine the state evolution by solving the Cauchy problem

$$\begin{cases} \dot{\varepsilon}(t) = p(t), \\ \dot{\sigma}(t) = \mathcal{F}\big(\varepsilon(t), \sigma(t), \operatorname{sgn} p(t)\big)p(t), \\ \varepsilon(0) = \varepsilon_0, \\ \sigma(0) = \sigma_0. \end{cases} \tag{9}$$

In particular, we have

$$\begin{aligned} \varepsilon(t) &= \varepsilon_0 + \int_0^t p(s)ds, \\ \sigma(t) &= \sigma_0 + \int_0^t \mathcal{F}\Big(\varepsilon(s), \sigma(s), \operatorname{sgn} p(s)\Big)p(s)ds, \end{aligned} \tag{10}$$

so that, by virtue of (8), we obtain

$$\varepsilon(d_p) = \varepsilon_0 + \int_0^{d_p} p(t)\,dt = \varepsilon_0 + \sum_{i=1}^{n} \int_{I_i^+} ds - \sum_{j=1}^{m} \int_{I_j^-} ds\,.$$

The *state transition function*, ρ, is defined as

$$\rho(\xi_0, p) = \xi_p,$$

where $\xi_p = (\varepsilon(d_p), \sigma(d_p))$ can be computed by means of (10) by letting $t = d_p$.

The mechanical work expended during the process p starting from ξ_0 is given by

$$w(\xi_0, p) = \int_0^{d_p} \sigma(t)\dot{\varepsilon}(t)dt = \int_0^{d_p} \sigma(t)p(t)dt. \tag{11}$$

Since $p \in \Pi$ is piecewise constant, this can be rewritten in the form of a Riemann-Stieltjes integral

$$w(\xi_0, p) = \int_0^{\varepsilon(d_p)} \sigma(t)\,d\varepsilon(t) = \sum_{i=1}^{n} \int_{I_i^+} \sigma(s)\,ds - \sum_{j=1}^{m} \int_{I_j^-} \sigma(s)\,ds, \tag{12}$$

where each addendum represents the area of a trapezoid between the segment $\sigma(s)$, $s \in I_i^+$ or $s \in I_i^-$, and the ε-axis. This geometrical representation of the work will be widely exploited throughout the paper in order to simplify calculations.

In the sequel, we show the complete controllability of the dynamical system (10) by proving that each state is accessible from and controllable at the origin $(0, 0)$. These are the contents of the following Lemmas 4.1 and 4.2, whose proofs are postponed and carried out within the Appendices.

Although estimates of the amount of work expended or absorbed during control processes are not needed in connection with accessibility and controllability, nevertheless we include them into the statements of these Lemmas. Indeed, they will be useful thereafter, in order to construct the minimum and maximum free energies. For instance, controllability at the origin $(0, 0)$ in Lemma 4.2 looks trivial, since it is apparent that *any* process that brings ε to 0 also drives σ to 0. Nevertheless, we are ultimately interested in choosing among others a process which maximizes the recovered work. This is why the control processes that appear within Lemmas 4.1 and 4.2 contain sawtooth-shaped paths whose amplitude decreases with the number n of their teeth. Actually, they turn out to be *almost optimal*, in the sense that

the minimum required work and the maximum recoverable work are respectively obtained in the limit as $n \to \infty$.

Henceforth, functions $f(\sigma)$ and $g(\xi)$ are convenient positive functions whose explicit expressions can be found into the Appendices.

Lemma 4.1 (Accessibility from the origin)**.** *Let $\bar{\mathcal{S}}_1 = \mathcal{S}_1 \cup \mathcal{P}_1$ and $\bar{\mathcal{S}}_2 = \mathcal{S}_2 \cup \mathcal{P}_2$. Starting from the origin $(0,0)$, each state $\xi \in \Xi$ can be reached by a suitable process. Indeed, the following results hold.*

(i) *For every state $\xi_1 = (\varepsilon_1, \sigma_1) \in \bar{\mathcal{S}}_1$ there exists a process $p^+ \in \Pi$, such that*

$$\rho((0,0), p^+) = \xi_1 \qquad \text{and} \qquad w((0,0), p^+) = \frac{\varepsilon_1 \sigma_1}{2} = \frac{1}{2}\alpha\, \varepsilon_1^2.$$

(ii) *For every state $\xi_* = (\varepsilon_*, \sigma_*) \in \mathcal{S}_*$ and for every $n \in \mathbb{N}$ there exists a process $p^+_{*n} \in \Pi$ such that*

$$\rho((0,0), p^+_{*n}) = \xi_* \qquad \text{and} \qquad w((0,0), p^+_{*n}) = \frac{1}{2}\sigma_*\varepsilon_* + \frac{1}{2\alpha} y(\alpha\varepsilon_* - \sigma_*) + \frac{1}{n} f(\sigma_*).$$

(iii) *For every state $\xi_2 = (\varepsilon_2, \sigma_2) \in \bar{\mathcal{S}}_2$ and for every $n \in \mathbb{N}$ there exists a process $p^+_{2n} \in \Pi$ such that*

$$\rho((0,0), p^+_{2n}) = \xi_2 \quad \text{and}$$
$$w((0,0), p^+_{2n}) = \frac{1}{2}\sigma_2\varepsilon_2 + \frac{1}{2\alpha} y(\alpha\varepsilon_2 - \sigma_2) - \frac{h(\alpha+\kappa)}{2\alpha\kappa}(\sigma_2 - y + h) + \frac{1}{n} f(y-h).$$

(iv) *For every state $\bar{\xi} = (\bar{\varepsilon}, \bar{\sigma}) \in \Xi_1 \cup \Xi_2$ and for every $n \in \mathbb{N}$ there exists a process $\bar{p}^+_n \in \Pi$ such that*

$$\rho((0,0), \bar{p}^+_n) = \bar{\xi} \quad \text{and}$$
$$w((0,0), \bar{p}^+_n) = \frac{1}{2}\bar{\sigma}\bar{\varepsilon} + \frac{1}{2\alpha} y(\alpha\bar{\varepsilon} - \bar{\sigma}) - \frac{1}{2\kappa}(y - \bar{\sigma})\Big[y\Big(1 + \frac{\kappa}{\alpha}\Big) - \kappa\bar{\varepsilon} - \bar{\sigma}\Big] + \frac{1}{n} f(\bar{\sigma}).$$

Lemma 4.2 (Controllability at the origin)**.** *Starting from each state $\xi \in \Xi$, the origin $(0,0)$ can be reached by any process p such that $\varepsilon(d_p) = 0$. In particular,*

(i) *For every state $\xi_1 = (\varepsilon_1, \sigma_1) \in \bar{\mathcal{S}}_1$ there exists a process $p^- \in \Pi$, such that*

$$\rho(\xi_1, p^-) = (0,0) \qquad \text{and} \qquad w(\xi_1, p^-) = -\frac{\varepsilon_1 \sigma_1}{2} = -\frac{1}{2}\alpha\, \varepsilon_1^2.$$

(ii) *For every state $\xi_* = (\varepsilon_*, \sigma_*) \in \mathcal{S}_*$ and for every $n \in \mathbb{N}$ there exists a process $p^-_{*n} \in \Pi$ such that*

$$\rho(\xi_*, p^-_{*n}) = (0,0) \qquad \text{and} \qquad w(\xi_*, p^-_{*n}) = -\frac{1}{2}\sigma_*\varepsilon_* - \frac{1}{2\alpha} y(\alpha\varepsilon_* - \sigma_*) + \frac{1}{n} f(\sigma_*).$$

(iii) *For every state $\xi_2 = (\varepsilon_2, \sigma_2) \in \bar{\mathcal{S}}_2$ and for every $n \in \mathbb{N}$ there exists a process $p^-_{2n} \in \Pi$ such that*

$$\rho(\xi_2, p^-_{2n}) = (0,0) \quad \text{and}$$
$$w(\xi_2, p^-_{2n}) = -\frac{1}{2}\sigma_2\varepsilon_2 - \frac{1}{2\alpha} y(\alpha\varepsilon_2 - \sigma_2) + \frac{h(\alpha+\kappa)}{2\alpha\kappa}(\sigma_2 - y + h) + \frac{1}{n} f(y-h).$$

(iv) *For every state $\bar{\xi} = (\bar{\varepsilon}, \bar{\sigma}) \in \Xi_1 \cup \Xi_2$ and for every $n \in \mathbb{N}$ there exists a process $\tilde{p}^-_n \in \Pi$ such that*

$$\rho(\bar{\xi}, \tilde{p}^-_n) = (0,0) \quad \text{and}$$
$$w(\bar{\xi}, \tilde{p}^-_n) = -\frac{1}{2}\bar{\sigma}\bar{\varepsilon} - \frac{1}{2\alpha} y(\alpha\bar{\varepsilon} - \bar{\sigma}) - \frac{\alpha\bar{\varepsilon} - \bar{\sigma}}{2(\alpha+\kappa)}\Big[y\Big(1 + \frac{\kappa}{\alpha}\Big) - \kappa\bar{\varepsilon} - \bar{\sigma}\Big] + \frac{1}{n} g(\bar{\xi}).$$

Collecting previous lemmas, we deduce the following result.

Theorem 4.3. *System (5)-(6) is completely ρ-controllable, that is to say, for any given ξ_1, $\xi_2 \in \Xi$ there exists a process $p \in \Pi$ such that $\rho(\xi_1, p) = \xi_2$.*

5. **Minimum and maximum free energies.** Since the absolute temperature enters the constitutive relations just as a parameter, the local Clausius-Duhem inequality reduces to the so-called *dissipation inequality*

$$\dot{\psi}(t) \leq \sigma(t)\,\dot{\varepsilon}(t), \tag{13}$$

where ψ is the free energy density per unit volume. In the purely elastic regime, beyond the yield limit, σ is a linear function of ε, $\sigma = \alpha\varepsilon$, and all deformation paths are reversible. As a consequence, the dissipation inequality holds as an equality

$$\dot{\psi}(t) = \alpha\,\varepsilon(t)\,\dot{\varepsilon}(t),$$

and the *elastic energy potential* $\psi : \Xi \to \mathbb{R}$ is uniquely determined up to a constant. Namely, assuming the normalizing condition $\psi(0,0) = 0$, it reads

$$\psi_e(\varepsilon, \sigma) = \frac{1}{2}\,\alpha\,\varepsilon^2. \tag{14}$$

On the contrary, because of the multi-valued relation between σ and ε, in the pseudo-elastic regime there exists an uncountable set of functions $\psi : \Xi \to \mathbb{R}$, all of which are normalized at $(0,0)$ and satisfy the dissipation inequality (13). They are referred to as *pseudo-elastic energy subpotentials* for the given dynamical system (see, for instance, [15]).

Definition 5.1. At a given temperature $\theta > \theta^*_{\mathcal{A}}$, a function $\psi : \Xi \to \mathbb{R}$ is said a mechanical subpotential of (5)-(6) if it satisfies the following conditions

(i) $\psi(0,0) = 0$;
(ii) for every $\xi_1, \xi_2 \in \Xi$ and $p \in \Pi$ such that $\rho(\xi_1, p) = \xi_2$,

$$\psi(\xi_1) - \psi(\xi_2) \leq w(\xi_1, p), \tag{15}$$

where $w(\xi_1, p)$ is defined by (11).

For further reference, we stress that a subpotential ψ needs not be continuous.

In the purely elastic regime, (15) holds as an equality and the mechanical energy potential (14) is strictly related to the expended mechanical work, in that

$$w((0,0), p) = \frac{1}{2}\,\sigma\varepsilon = \psi_e.$$

Furthermore, we denote by Ψ the set of all subpotentials $\psi : \Xi \to \mathbb{R}$ and we let

$$\overleftarrow{\Pi}_\xi = \{p \in \Pi : \rho((\varepsilon,\sigma), p) = (0,0)\}, \qquad \overrightarrow{\Pi}_\xi = \{p \in \Pi : \rho((0,0), p) = (\varepsilon,\sigma)\},$$

where $\xi = (\varepsilon, \sigma)$. Since system (5)-(6) is completely controllable, $\overleftarrow{\Pi}_\xi$ and $\overrightarrow{\Pi}_\xi$ are non-empty sets. This is enough to conclude (see [15]) that there exist the minimum and maximum free energy subpotentials, denoted by $\psi_{\mathrm{m}}, \psi_{\mathrm{M}}$, and defined as

$$\psi_{\mathrm{m}}(\xi) = \sup_{p \in \overleftarrow{\Pi}_\xi} [-w(\xi, p)] = -\inf_{p \in \overleftarrow{\Pi}_\xi} w(\xi, p), \tag{16}$$

$$\psi_{\mathrm{M}}(\xi) = \inf_{p \in \overrightarrow{\Pi}_\xi} w((0,0), p). \tag{17}$$

The function ψ_{m} represents the maximum amount of work which may be extracted from the system when moving from $\xi = (\varepsilon, \sigma)$ to $(0,0)$, whereas ψ_{M} represents the

minimum amount of storage which is required to supply the system when attaining $\xi = (\varepsilon, \sigma)$ from $(0,0)$. As proved in [15], the set Ψ is convex and the following relation holds for any subpotential $\psi \in \Psi$,

$$\psi_{\rm m} \le \psi \le \psi_{\rm M}.$$

By paralleling [2] and taking Lemmas 4.1-4.2 into account, we deduce the explicit expression of the minimum and maximum free energies. Indeed we have

$$\psi_{\rm m}(\varepsilon,\sigma)=\begin{cases} \dfrac{\sigma\varepsilon}{2} & \text{if } (\varepsilon,\sigma)\in\bar{\mathcal{S}}_1\\[2mm] \dfrac{\sigma\varepsilon}{2}+\dfrac{y(\alpha\varepsilon-\sigma)}{2\alpha} & \text{if } (\varepsilon,\sigma)\in\mathcal{S}_*\\[2mm] \dfrac{\sigma\varepsilon}{2}+\dfrac{y(\alpha\varepsilon-\sigma)}{2\alpha}-\dfrac{h(\alpha+\kappa)}{2\alpha\kappa}(\sigma-y+h) & \text{if } (\varepsilon,\sigma)\in\bar{\mathcal{S}}_2\\[2mm] \dfrac{\sigma\varepsilon}{2}+\dfrac{y(\alpha\varepsilon-\sigma)}{2\alpha}+\dfrac{\alpha\varepsilon-\sigma}{2(\alpha+\kappa)}\Big[y\Big(1+\dfrac{\kappa}{\alpha}\Big)-\kappa\varepsilon-\sigma\Big] & \text{if } (\varepsilon,\sigma)\in\Xi_1\cup\Xi_2. \end{cases}$$

After some manipulations and remembering the definitions of $\bar{\mathcal{S}}_1$, $\bar{\mathcal{S}}_2$ and $\mathcal{S}_*$, $\psi_{\rm m}$ takes the following compact form on the positive major loop Ξ.

Proposition 1. *The minimum free energy $\psi_{\rm m}$ can be rewritten in the form*

$$\psi_{\rm m}(\varepsilon,\sigma)=\frac{1}{2}\sigma\varepsilon+\frac{y}{\alpha}(\alpha\varepsilon-\sigma)-\frac{\alpha\varepsilon-\sigma}{2(\alpha+\kappa)}(\kappa\varepsilon+\sigma)\,,\qquad(\varepsilon,\sigma)\in\Xi\,. \tag{18}$$

In addition, from Lemma 4.1 it follows

Proposition 2. *The maximum free energy takes the same values of $\psi_{\rm m}$ on the skeleton curve $\mathcal{S}$, and*

$$\psi_{\rm M}(\varepsilon,\sigma)=\begin{cases}\psi_{\rm m}(\varepsilon,\sigma) & \text{if } (\varepsilon,\sigma)\in\mathcal{S}\\ \psi_{\rm m}(\varepsilon,\sigma)+\chi(\varepsilon,\sigma) & \text{if } (\varepsilon,\sigma)\in\Xi_1\cup\Xi_2,\end{cases}$$

where $\chi(\varepsilon,\sigma)$ is given by

$$\chi(\varepsilon,\sigma)=\frac{\alpha}{2\kappa(\alpha+\kappa)}\Big[y\Big(1+\frac{\kappa}{\alpha}\Big)-\kappa\varepsilon-\sigma\Big]^2. \tag{19}$$

Remark 1. Notice that the minimum free energy $\psi_{\rm m}$ is continuous on Ξ, whereas $\psi_{\rm M}$ is discontinuous. In addition, both of them are independent of h and depend on θ only through y, as given in (1). Accordingly, for all temperatures $\theta > \theta^*_{\mathcal{A}}$, these energy expressions are defined on the region (cf. Fig. 9)

$$\mathcal{Z}^+=\{(\varepsilon,\sigma)\in\mathbb{R}^+\times\mathbb{R}^+:\,\sigma\le\alpha\varepsilon\le\sigma+\alpha\varepsilon_t\}\,,\qquad \varepsilon_t=h\frac{\alpha+\kappa}{\alpha\kappa}\,.$$

For further reference, we define the *free enthalpy* (or Gibbs free energy) as $\zeta(\varepsilon,\sigma)=\psi(\varepsilon,\sigma)-\varepsilon\sigma$. In this connection, for all $(\varepsilon,\sigma)\in\mathcal{Z}^+$ we have

$$\zeta_{\rm m}(\varepsilon,\sigma)=\psi_{\rm m}(\varepsilon,\sigma)-\varepsilon\sigma=-\frac{1}{2}\sigma\varepsilon+\frac{y}{\alpha}(\alpha\varepsilon-\sigma)-\frac{\alpha\varepsilon-\sigma}{2(\alpha+\kappa)}(\kappa\varepsilon+\sigma)\,. \tag{20}$$

6. **An application to the Ginzburg-Landau Theory.** In the whole pseudo-elastic region, where $\theta > \theta^*_{\mathcal{A}}$ and $\sigma\,\varepsilon \geq 0$ (cf. Fig. 1), we first introduce a phase-field parameter, which describes the austenite-martensite transformation in connection with phenomenological variables. Our goal is to express the free energy $\psi_{\rm m}$ and free enthalpy $\zeta_{\rm m}$ as functions of this parameter. To this end, we introduce the additive decomposition of ε into an *elastic deformation*, ε_e, and a *plastic deformation*, ε_p, as well as in elasto-plasticity. Namely, according to the assumption of small deformations, $\varepsilon = \varepsilon_e + \varepsilon_p$, and

$$\varepsilon_e = \frac{1}{\alpha}\sigma, \qquad \varepsilon_p = \varepsilon - \frac{1}{\alpha}\sigma, \qquad |\varepsilon_p| \leq \varepsilon_t,$$

which means that the stress is contributed by the elastic deformation, only. In this framework, the minimum free energy and enthalpy take the alternative forms

$$\begin{aligned} \bar{\psi}_{\rm m}(\varepsilon_p, \sigma) &= \frac{1}{2\alpha}\sigma^2 + y\varepsilon_p - \frac{h}{2\varepsilon_t}\varepsilon_p^2\,, \\ \bar{\zeta}_{\rm m}(\varepsilon_p, \sigma) &= -\frac{1}{2\alpha}\sigma^2 + (y-\sigma)\varepsilon_p - \frac{h}{2\varepsilon_t}\varepsilon_p^2\,. \end{aligned} \tag{21}$$

At this point, we introduce the martensite concentration φ as an order parameter, which encodes the atomic configurations through the transformation. To account for both the oriented phases, $\mathcal{M}^+$ and $\mathcal{M}^-$, we conventionally assume that a positive value of φ represents the concentration of martensite $\mathcal{M}^+$, whereas the absolute value of a negative φ represents the concentration of martensite $\mathcal{M}^-$. Accordingly, $\varphi = 0$ when the material is totally in the austenitic phase, and $\varphi = +1$ ($\varphi = -1$) when the material is totally in the martensitic phase $\mathcal{M}^+$ ($\mathcal{M}^-$). Of course, a consistency condition is required, namely φ and σ must have the same sign, $\varphi\,\sigma \geq 0$.

If we limit our attention to the positive-oriented martensite $\mathcal{M}^+$, we are allowed to assume, as customary, that the plastic deformation is a (possibly nonlinear) function of φ,

$$\varepsilon_p = \varepsilon_t \gamma(\varphi)\,,$$

where γ is a monotone increasing, positive function on $(0,1)$ such that

$$\gamma(0) = 0\,, \qquad \gamma(1) = 1\,, \qquad \gamma'(0) = \gamma'(1) = 0\,, \qquad \gamma''(0) > 0\,, \qquad \gamma''(1) < 0.$$

The choice of γ reflects the phenomenological relation between the martensite concentration and the plastic deformation and can be experimentally tested. By collecting the previous assumptions we have

$$\varepsilon = \varepsilon_e + \varepsilon_p = \frac{1}{\alpha}\sigma + \varepsilon_t \gamma(\varphi).$$

This statement is exactly that given in [9, eq.(6)] and in [4, eq.(3)], provided that $\varepsilon_0 = 4\varepsilon_t$, $\lambda = 1/\alpha$ and $\gamma = 4G$. Unlike those papers, however, here the expression of the Gibbs free energy will not be prescribed *a priori* (see § 4), but computed *a posteriori*, according to the given stress-strain evolution model.

Since the pair of variables (φ, σ) is perfectly equivalent to (ε, σ), both the minimum free energy and the enthalpy can be represented with respect to (φ, σ). The region $\mathcal{Z}^+$ transforms into the corresponding set $\mathcal{R}^+ = [0,1] \times \mathbb{R}^+$, so that we obtain

$$\tilde{\zeta}_{\rm m}(\varphi, \sigma) = -\frac{1}{2\alpha}\sigma^2 + (y-\sigma)\varepsilon_t\gamma(\varphi) - \frac{h}{2}\varepsilon_t\gamma^2(\varphi)\,.$$

In order to represent both martensitic phases, $\mathcal{M}^+$ and $\mathcal{M}^-$, we let Γ be the symmetric extension of γ on $[-1,1]$, namely, $\Gamma(\varphi) = \gamma(|\varphi|)$. Accordingly, $\varepsilon_p = 0$

in the pure austenite phase $\varphi = 0$, and $\varepsilon_p = \pm\varepsilon_t$ in the pure martensite phases $\varphi = \pm 1$. For definiteness, we can choose either a trigonometric or a polynomial function (see Fig. 10),

$$\Gamma_1(\varphi) = \frac{1}{2}(1 - \cos \pi\varphi)\,, \qquad \Gamma_2 = \varphi^2(2 - \varphi^2)\,, \qquad \varphi \in [-1, 1]\,.$$

A more general fourth-order polynomial is scrutinized in [9, eq.(11) and Fig. 4].

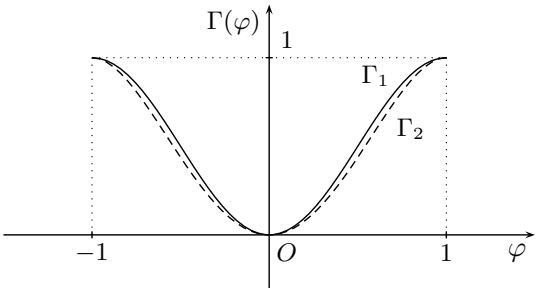

FIGURE 10. The graphs of Γ_1 (solid) and Γ_2 (dashed) on $(-1, 1)$.

In order to extend all the energy expressions to the whole pseudo-elastic range,

$$\mathcal{R} = \{(\varphi, \sigma) \in [-1, 1] \times \mathbb{R} : \varphi\,\sigma \geq 0\}\,, \tag{22}$$

we observe that the symmetry requirement $\tilde{\zeta}(-\varphi, -\sigma) = \tilde{\zeta}(\varphi, \sigma)$ implies

$$\tilde{\zeta}_{\rm m}(\varphi, \sigma) = -\frac{1}{2\alpha}\sigma^2 - \varepsilon_t|\sigma|\Gamma(\varphi) + \varepsilon_t\left(y - \frac{h}{2}\Gamma(\varphi)\right)\Gamma(\varphi)\,,$$

which is consistent with [9, eq.(7)] and admits a three-dimensional generalization.

Now, this result can be exploited in connection with the well-known Ginzburg-Landau equation

$$\dot{\varphi} = -\tau(\partial_\varphi\zeta - \nabla \cdot \partial_{\nabla\varphi}\zeta)\,, \qquad \tau > 0\,.$$

When deformations and density variations are allowed, it involves the *total free enthalpy* (rather than the total free energy): $\zeta(\varphi, \nabla\varphi, \sigma) = \tilde{\zeta}(\varphi, \sigma) + \frac{1}{2}\mu|\nabla\varphi|^2$, where the last term represents the interface energy and vanishes in spatially homogeneous processes. Then, assuming $\tilde{\zeta} = \tilde{\zeta}_{\rm m}$ and applying the expression of the minimum free enthalpy $\tilde{\zeta}_{\rm m}$, the Ginzburg-Landau equation takes the explicit form

$$\dot{\varphi} = -\tau[\partial_\varphi\tilde{\zeta}_{\rm m}(\varphi, \sigma) - \mu\Delta\varphi] = -\tau\varepsilon_t\big[y - |\sigma| - h\Gamma(\varphi)\big]\Gamma'(\varphi) + \tau\mu\Delta\varphi. \tag{23}$$

According to the Ginzburg-Landau theory, at a fixed stress σ and temperature $\theta > \theta^*_{\mathcal{A}}$ the local minima of $\tilde{\zeta}_{\rm m}$ on $\mathcal{R}$ represent stable equilibria for the related phase-field model. The following theorem gives a characterization of these points.

Theorem 6.1. *For any given $y > h > 0$, the nature of the stationary points of $\tilde{\zeta}_{\rm m}(\cdot, \sigma)$ depends on σ as follows (see Fig. 11):*

- *$\varphi = 0$ is a local minimum provided that $|\sigma| < y$ and a maximum otherwise;*
- *$\varphi = 1$ is a local minimum provided that $\sigma > y - h$ and a maximum otherwise;*
- *$\varphi = -1$ is a local minimum provided that $\sigma < -y + h$ and a maximum otherwise;*
- *$\varphi = \tilde{\varphi}_+$ is a local maximum whenever it exists, namely when $y - h < \sigma < y$;*
- *$\varphi = \tilde{\varphi}_-$ is a local maximum whenever it exists, namely when $-y < \sigma < -y + h$.*

Proof. First, we observe that any local minimum satisfies the following relations

$$\partial_\varphi \tilde{\zeta}_{\rm m}(\varphi,\sigma) = \varepsilon_t\big[y-|\sigma|-h\Gamma(\varphi)\big]\Gamma'(\varphi) = 0\,,$$
$$\partial^2_\varphi \tilde{\zeta}_{\rm m}(\varphi,\sigma) = \varepsilon_t\big[y-|\sigma|-h\Gamma(\varphi)\big]\Gamma''(\varphi) - h\varepsilon_t[\Gamma'(\varphi)]^2 > 0.$$

For all $\varphi\in[-1,1]$ we have $y-h\Gamma(\varphi)\geq y-h>0$ and

$$y-|\sigma|-h\Gamma(\varphi)\begin{cases} >0 & \text{if } \ |\sigma|<y-h,\\ <0 & \text{if } \ |\sigma|>y.\end{cases}$$

Otherwise, when $y-h<|\sigma|<y$, this factor vanishes at $\tilde\varphi_-,\tilde\varphi_+\in(-1,1)$, where $\tilde\varphi_\pm=\pm\,\gamma^{-1}\left(\frac{y-|\sigma|}{h}\right)$. As a consequence, the stationary points of $\tilde\zeta_{\rm m}(\cdot,\sigma)$ are

$$\begin{aligned} \varphi&=-1,0,1 && \text{if } \ |\sigma|\leq y-h,\\ \varphi&=-1,\tilde\varphi_-,0,\tilde\varphi_+,1 && \text{if } \ y-h<|\sigma|<y,\\ \varphi&=-1,0,1 && \text{if } \ |\sigma|\geq y.\end{aligned}$$

Then, taking into account the constraint $\sigma\,\varphi\geq 0$ and the relations

$$\partial^2_\varphi\tilde\zeta_{\rm m}(0,\sigma)=\varepsilon_t\big[y-|\sigma|\big]\Gamma''(0)\,,\quad \partial^2_\varphi\tilde\zeta_{\rm m}(\pm1,\sigma)=\varepsilon_t\big[y-|\sigma|-h\big]\Gamma''(\pm1)\,,$$
$$\partial^2_\varphi\tilde\zeta_{\rm m}(\tilde\varphi_\pm,\sigma)=-h\varepsilon_t[\Gamma'(\tilde\varphi_\pm)]^2\,,$$

the desired result follows. □

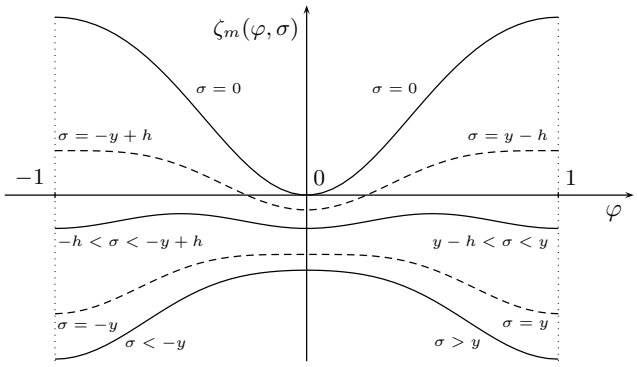

FIGURE 11. The graphs of $\tilde\zeta_{\rm m}(\cdot,\sigma)$, at different values of σ, when $\Gamma=\Gamma_1$.

Remark 2. Only pure phases represent stable equilibria for the G-L equation (see solid lines in Fig. 12). Nevertheless, inside the major loop there exists a set of unstable (or "metastable") equilibrium states, which are a suitable mixture of the pure phases. In connection with this feature, our model is very close to that proposed and scrutinized in [12].

Remark 3. The Ginzburg-Landau equation derived here is a special case of that presented in [3, eq.7] (see also [4]), namely

$$\beta\dot\varphi=\kappa\Delta\varphi-2\theta_0F'(\varphi)-[\hat\theta-6\varepsilon_0|\sigma|]G'(\varphi)\,,$$

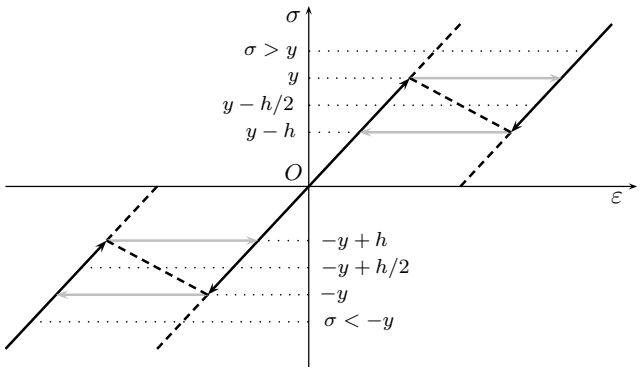

FIGURE 12. Stable (solid) and unstable (dashed) equilibrium branches.

Indeed, (23) can be obtained from it by choosing $\varepsilon_0 = \varepsilon_t$, $\kappa = \mu$ and

$$\beta = \frac{1}{\tau}\,, \quad G(\varphi) = \frac{1}{6}\Gamma(\varphi)\,, \quad F(\varphi) = -\frac{1}{12}\Gamma^2(\varphi)\,, \quad \hat{\theta} = 6y\,\varepsilon_t\,, \quad \theta_0 = 3h\,\varepsilon_t.$$

As a consequence of [3, Theorem 3.1], any solution φ to (23) verifies the bound

$$|\varphi(x,t)| \le 1, \qquad \text{for almost all } (x,t)\,,$$

provided that the same bound is satisfied by the initial datum $\varphi_0 = \varphi(x,0)$.

Appendix A. Proof of Lemma 4.1.

(i) Let $\xi_1 = (\varepsilon_1, \sigma_1) \in \bar{\mathcal{S}}_1$. In particular, $\sigma_1 = \alpha\varepsilon_1$, with $0 \le \varepsilon_1 \le y/\alpha$. In order to prove the statement, we choose the process p_1^+ of duration $d^+ = \varepsilon_1$, namely

$$p_1^+(t) = 1, \quad t \in [0, \varepsilon_1).$$

In view of equations (6) and (10), we deduce

$$\varepsilon(d^+) = \int_0^{\varepsilon_1} p_1^+(s)ds = \varepsilon_1, \qquad \sigma(d^+) = \int_0^{\varepsilon_1} \alpha\, p_1^+(s)ds = \alpha\varepsilon_1 = \sigma_1,$$

which proves the first part of the item.

From the direct application of (11) it follows that

$$w((0,0), p_1^+) = \int_0^{\varepsilon_1} \alpha\,\varepsilon(s)\,\dot{\varepsilon}(s)\,ds = \frac{1}{2}\alpha\,\varepsilon_1^2.$$

By virtue of (12), this amount coincides with the area of the grey-colored region in Fig. 13,

$$w((0,0), p_1^+) = \int_0^{\varepsilon_1} \sigma(s)\,ds = \frac{1}{2}\sigma_1\varepsilon_1,$$

which completes the proof of the first item.

(ii) Let $\xi_* = (\varepsilon_*, \sigma_*) \in \mathcal{S}_*$. We first observe that $y/\alpha < \varepsilon_* < y/\alpha + h/\kappa$ and

$$\sigma_* = -\kappa\varepsilon_* + y(1 + \kappa/\alpha).$$

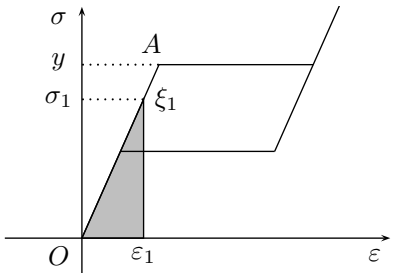

FIGURE 13. Work required to reach ξ_1 starting from the origin.

For later convenience, we let

$$a_n = \frac{1}{n\alpha}\left(\alpha\varepsilon_* - \sigma_*\right), \quad b_n = \frac{1}{n\alpha}(y-\sigma_*), \quad a_n + b_n = \frac{1}{n\alpha}\left(\alpha\varepsilon_* + y - 2\sigma_*\right). \tag{24}$$

In particular, when $\xi_* = D$, then $\varepsilon_* = y/\alpha + h/\kappa$, $\sigma_* = y - h$ and

$$a_n = \frac{h}{n}\left(\frac{1}{\alpha} + \frac{1}{\kappa}\right), \qquad b_n = \frac{h}{n\alpha}, \qquad a_n + b_n = \frac{h}{n}\left(\frac{2}{\alpha} + \frac{1}{\kappa}\right). \tag{25}$$

Now, we choose $p^+_{*n} = p^+ * p^+_n$, where

$$p^+(t) = 1, \quad t \in [0, y/\alpha), \tag{26}$$

and

$$p^+_n(t) = \begin{cases} +1 & t \in I^+_j, \quad j = 0, 1, ..., n-1 \\ -1 & t \in I^-_j, \quad j = 0, 1, ..., n-1, \end{cases} \tag{27}$$

$I^+_j = \big[j(a_n+b_n), j(a_n+b_n)+a_n\big), \quad I^-_j = \big[j(a_n+b_n)+a_n, (j+1)(a_n+b_n)\big)$.

In the sequel, p^+_n will be referred to as *"sawtooth" process*. The duration of p^+_{*n} is given by

$$d^+_* = y/\alpha + \sum_{j=0}^{n-1} |I^+_j| + \sum_{j=0}^{n-1} |I^-_j| = y/\alpha + n(a_n+b_n) = \varepsilon_* + 2\left(y - \sigma_*\right)/\alpha$$

and in view of equations (6) and (10) we deduce

$$\begin{aligned} \varepsilon(d^+_*) &= \int_0^{d^+_*} p^+_{*n}(s)ds = \int_0^{y/\alpha} ds + \sum_{j=0}^{n-1}\int_{I^+_j} ds - \sum_{j=0}^{n-1}\int_{I^-_j} ds \\ &= \frac{y}{\alpha} + n\,a_n - n\,b_n = \varepsilon_*, \\ \sigma(d^+_*) &= \int_0^{d^+_*} \dot\sigma(s)ds = \int_0^{y/\alpha} \alpha\, ds - \sum_{j=0}^{n-1}\int_{I^-_j} \alpha\, ds = y - n\alpha\, b_n = \sigma_*, \end{aligned}$$

which proves the first part of the item. Finally, from (12) and (27), we have

$$w((0,0), p^+_{*n}) = \int_0^{y/\alpha} \sigma(s)\, ds + \sum_{j=0}^{n-1}\int_{I^+_j}\left[y - \frac{j}{n}(y-\sigma_*)\right] ds - \sum_{j=0}^{n-1}\int_{I^-_j} \sigma(s)\, ds.$$

This value represents the area of the grey-colored region in Fig. 14 and can be easily computed by adding the areas of the triangle OAA', the trapezoid beneath $A\xi_*$ and the saw-shaped polygon above the same segment:

$$\frac{1}{2\alpha}y^2 + \frac{1}{2}(y+\sigma_*)\Big(\varepsilon_* - \frac{y}{\alpha}\Big) + \frac{1}{2n}(y-\sigma_*)^2\Big(\frac{1}{\kappa}+\frac{1}{\alpha}\Big).$$

Some simple arrangements and the position

$$f(\sigma_*) = \frac{1}{2}(y-\sigma_*)^2\Big(\frac{1}{\kappa}+\frac{1}{\alpha}\Big) \tag{28}$$

yield the final expression of the work expended along the process p^+_{*n},

$$w((0,0),p^+_{*n}) = \frac{1}{2}\sigma_*\varepsilon_* + \frac{1}{2\alpha}y(\alpha\varepsilon_* - \sigma_*) + \frac{1}{n}f(\sigma_*).$$

Here, by virtue of (A), σ_* can be expressed as a function of ε_*, namely

$$w((0,0),p^+_{*n}) = -\frac{\kappa\varepsilon_*^2}{2} + \varepsilon_* y\Big(1+\frac{\kappa}{\alpha}\Big) - \frac{y^2}{2\alpha}\Big(1+\frac{\kappa}{\alpha}\Big) + \frac{\kappa^2}{2n}\Big(\varepsilon_* - \frac{y}{\alpha}\Big)^2\Big(\frac{1}{\kappa}+\frac{1}{\alpha}\Big).$$

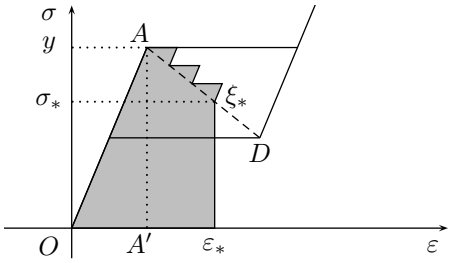

FIGURE 14. Work required to reach ξ_* starting from the origin ($n = 3$).

(iii) Let $\xi_2 = (\varepsilon_2, \sigma_2) \in \mathcal{S}_2$. As a consequence, $\varepsilon_2 > y/\alpha + h/\kappa$ and

$$\sigma_2 = \alpha\varepsilon_2 - h(1+\alpha/\kappa). \tag{29}$$

In order to prove the statement, we choose $p^+_{2n} = p^+ * p^+_n * p^+_2$, where p^+ is given by (26), p^+_n is the sawtooth process obtained from (27) with a_n, b_n given by (25), and

$$p^+_2(t) = 1, \quad t \in [0, \varepsilon_2 - y/\alpha - h/\kappa).$$

The total duration of p^+_{2n} is given by

$$d^+_2 = \frac{y}{\alpha} + \sum_{j=0}^{n-1}|I^+_j| + \sum_{j=0}^{n-1}|I^-_j| + \varepsilon_2 - \Big(\frac{y}{\alpha}+\frac{h}{\kappa}\Big) = \varepsilon_2 + \frac{2h}{\alpha}.$$

In view of equations (6) and (10), by virtue of (25) and (29) we deduce

$$\begin{aligned}\varepsilon(d_2^+) &= \int_0^{y/\alpha} ds + \sum_{j=0}^{n-1}\int_{I_j^+} ds - \sum_{j=0}^{n-1}\int_{I_j^-} ds + \int_0^{\varepsilon_2-y/\alpha-h/\kappa} ds\\ &= n\,a_n - n\,b_n + \varepsilon_2 - \frac{h}{\kappa} = h\left(\frac{1}{\alpha}+\frac{1}{\kappa}\right) - \frac{h}{\alpha} + \varepsilon_2 - \frac{h}{\kappa} = \varepsilon_2,\\ \sigma(d_2^+) &= \int_0^{y/\alpha} \alpha\, ds - \sum_{j=0}^{n-1}\int_{I_j^-} \alpha\, ds + \int_0^{\varepsilon_2-y/\alpha-h/\kappa} \alpha\, ds\\ &= y - n\alpha\, b_n + \alpha\varepsilon_2 - y - h\alpha/\kappa = \alpha\varepsilon_2 - h(1+\alpha/\kappa) = \sigma_2,\end{aligned}$$

which proves the first part of the item.

Finally, the work required to reach ξ_2 starting from the origin is represented by the area of the grey-colored region in Fig. 15. It can be easily computed by adding the areas of the triangle OAA', the trapezoid $ADD'A'$, the trapezoid beneath the segment $D\xi_2$ and the saw-shaped polygon above the segment AD:

$$\frac{1}{2\alpha}y^2 + \frac{h}{2\kappa}(2y-h) + \frac{1}{2}(\sigma_2+y-h)\Big(\varepsilon_2 - \frac{y}{\alpha} - \frac{h}{\kappa}\Big) + \frac{1}{2n}h^2\Big(\frac{1}{\kappa}+\frac{1}{\alpha}\Big).$$

Some simple arrangements and the position (28) yield

$$w((0,0),p_{2n}^+) = \frac{1}{2}\sigma_2\varepsilon_2 + \frac{1}{2\alpha}y(\alpha\varepsilon_2-\sigma_2) - \frac{h(\alpha+\kappa)}{2\alpha\kappa}(\sigma_2-y+h) + \frac{1}{n}f(y-h),$$

which proves the second part of this item. In terms of ε_2, only,

$$w((0,0),p_{2n}^+) = \frac{1}{2}\alpha\,\varepsilon_2^2 - h\varepsilon_2(1+\frac{\alpha}{\kappa}) + \frac{h}{2\alpha}(1+\frac{\alpha}{\kappa})(2y+\frac{h}{k}) + \frac{1}{n}f(y-h).$$

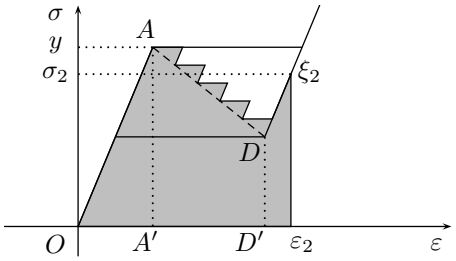

FIGURE 15. Work required to reach ξ_2 starting from the origin ($n=5$).

(iv) Let $\bar\xi = (\bar\varepsilon,\bar\sigma) \in \Xi_1 \cup \Xi_2$. We first observe that $\bar\sigma + \kappa\bar\varepsilon - h(1+\kappa/\alpha) < 0$ when $\bar\xi \in \Xi_1$ and $\bar\sigma + \kappa\bar\varepsilon - h(1+\kappa/\alpha) > 0$ when $\bar\xi \in \Xi_2$. Let ξ_* be the point of the segment AD such that $\sigma_* = \bar\sigma$ and

$$\varepsilon_* = -\bar\sigma/\kappa + y(1/\alpha + 1/\kappa). \tag{30}$$

Now we choose $\bar p_n^+ = p^+ * p_n^+ * \bar p$, where p^+ is given by (26), p_n^+ is the sawtooth process obtained from (27) with a_n, b_n given by (24), and

$$\bar p(t) = \begin{cases} -1 & t \in [0, \varepsilon_* - \bar\varepsilon), \quad \text{if } \bar\xi \in \Xi_1\\ +1 & t \in [0, \bar\varepsilon - \varepsilon_*), \quad \text{if } \bar\xi \in \Xi_2.\end{cases}$$

The duration of $\bar{p}_n^+$ is given by

$$\begin{aligned}\bar{d}^+ &= y/\alpha + \sum_{j=0}^{n-1} |I_j^+| + \sum_{j=0}^{n-1} |I_j^-| + |\bar{\varepsilon} - \varepsilon_*| = \varepsilon_* + 2\,(y - \sigma_*)\,/\alpha + |\bar{\varepsilon} - \varepsilon_*| \\ &= -\bar{\sigma}/\kappa + y(1/\alpha + 1/\kappa) + 2\,(y - \bar{\sigma})\,/\alpha + |\bar{\varepsilon} + \bar{\sigma}/\kappa - y(1/\alpha + 1/\kappa)|.\end{aligned}$$

In view of equations (6) and (10), by virtue of (A) and (24) we deduce

$$\begin{aligned}\varepsilon(\bar{d}^+) &= \int_0^{y/\alpha} ds + \sum_{j=0}^{n-1} \int_{I_j^+} ds - \sum_{j=0}^{n-1} \int_{I_j^-} ds + \int_0^{\bar{\varepsilon}-\varepsilon_*} ds \\ &= \frac{y}{\alpha} + n\,a_n - n\,b_n + \bar{\varepsilon} - \varepsilon_* = \bar{\varepsilon}, \\ \sigma(\bar{d}^+) &= \int_0^{y/\alpha} \alpha\, ds - \sum_{j=0}^{n-1} \int_{I_j^-} \alpha\, ds = y - n\alpha\, b_n = \sigma_* = \bar{\sigma},\end{aligned}$$

which proves the first part of the item. Finally, from (12) and (27), we have

$$\begin{aligned}w((0,0),\bar{p}_n^+) \;=\; & \int_0^{y/\alpha} \sigma(s)\, ds + \sum_{j=0}^{n-1} \int_{I_j^+} \left[y - \frac{j}{n}(y - \sigma_*)\right] ds \\ & - \sum_{j=0}^{n-1} \int_{I_j^-} \sigma(s)\, ds + \int_0^{\bar{\varepsilon}-\varepsilon_*} \sigma_*\, ds.\end{aligned}$$

This value represents the area of the grey-colored region in Fig. 16 and can be easily computed by adding the areas of the triangle OAA', the trapezoid beneath $A\xi_*$, the saw-shaped polygon above the same segment and by adding or subtracting the area of the rectangle beneath the segment $\xi_*\bar{\xi}$ depending on the position of $\bar{\xi}$:

$$\frac{1}{2\alpha}y^2 + \frac{1}{2}(y + \bar{\sigma})\Big(\varepsilon_* - \frac{y}{\alpha}\Big) + \frac{1}{2n}(y - \bar{\sigma})^2\Big(\frac{1}{\kappa} + \frac{1}{\alpha}\Big) + \bar{\sigma}(\bar{\varepsilon} - \varepsilon_*).$$

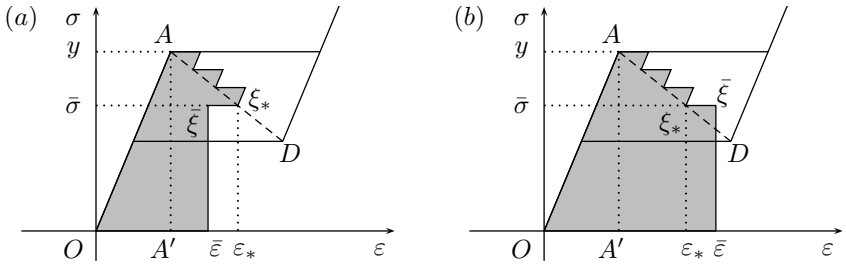

FIGURE 16. Work required to reach $\bar{\xi}$ starting from the origin ($n = 3$), when: (a) $\bar{\xi} \in \Xi_1$, (b) $\bar{\xi} \in \Xi_2$.

Some simple arrangements and the use of (28), (30) yield

$$w((0,0),\bar{p}_n^+) = \frac{\bar{\sigma}\bar{\varepsilon}}{2} + \frac{y(\alpha\bar{\varepsilon} - \bar{\sigma})}{2\alpha} - \frac{y - \bar{\sigma}}{2\kappa}\Big[y\Big(1 + \frac{\kappa}{\alpha}\Big) - \kappa\bar{\varepsilon} - \bar{\sigma}\Big] + \frac{1}{n}f(\bar{\sigma}).$$

Appendix B. **Proof of Lemma 4.2.**

(i) By paralleling the item (i) of Lemma 4.1, we choose

$$p_1^-(t) = -1, \quad t \in [0, \varepsilon_1),$$

and, in view of equations (6) and (10), we deduce

$$\varepsilon(d^-) = \varepsilon_1 + \int_0^{\varepsilon_1} p_1^-(s)ds = 0,$$
$$\sigma(d^-) = \sigma_1 + \int_0^{\varepsilon_1} \alpha\, p_1^-(s)ds = \sigma_1 - \alpha\varepsilon_1 = 0.$$

Then, the amount of work which is recovered during the process p_1^- coincides with the negative of the grey-colored area in Fig. 13, namely

$$w(\xi_1, p_1^-) = -\frac{1}{2}\alpha\,\varepsilon_1^2 = -\frac{1}{2}\sigma_1\varepsilon_1.$$

(ii) By paralleling the item (ii) of Lemma 4.1, we choose $p_{*n}^- = p_n^- * p^-$, where

$$p^-(t) = -1, \quad t \in [0, y/\alpha), \tag{31}$$

$$p_n^-(t) = \begin{cases} -1 & t \in I_j^-, \quad j = 0, 1, ..., n-1 \\ +1 & t \in I_j^+, \quad j = 0, 1, ..., n-1. \end{cases} \tag{32}$$

The intervals I_j^- and I_j^+ are defined as in (27) and the duration $d_*^- = d_*^+$. In view of equations (6) and (10) we deduce

$$\varepsilon(d_*^-) = \varepsilon_* - \sum_{j=0}^{n-1}\int_{I_j^-} ds + \sum_{j=0}^{n-1}\int_{I_j^+} ds - \int_0^{y/\alpha} ds = \varepsilon_* - n\,b_n + n\,a_n - \frac{y}{\alpha} = 0,$$
$$\sigma(d_*^-) = \sigma_* + \sum_{j=0}^{n-1}\int_{I_j^-} \alpha\, ds - \int_0^{y/\alpha} \alpha\, ds = \sigma_* + n\alpha\, b_n - y = 0.$$

Finally, from (12), we have

$$w(\xi^*, p_{*n}^-) = -\sum_{j=0}^{n-1}\int_{I_j^-}\left[y - \frac{n-j}{n}(y - \sigma_*)\right]ds + \sum_{j=0}^{n-1}\int_{I_j^+}\sigma(s)ds - \int_0^{y/\alpha}\sigma(s)ds.$$

This value represents the negative of the area of the grey-colored region in Fig. 17. Such area can be easily computed by adding the areas of the triangle OAA', the trapezoid beneath $A\xi_*$ and then subtracting the area of the saw-shaped polygon above the same segment:

$$\frac{1}{2\alpha}y^2 + \frac{1}{2}(y + \sigma_*)\Big(\varepsilon_* - \frac{y}{\alpha}\Big) - \frac{1}{2n}(y - \sigma_*)^2\Big(\frac{1}{\kappa} + \frac{1}{\alpha}\Big).$$

Some simple arrangements yield the final expression of the work recovered along the process p_{*n}^-,

$$w(\xi_*, p_{*n}^-) = -\frac{1}{2}\sigma_*\varepsilon_* - \frac{1}{2\alpha}y(\alpha\varepsilon_* - \sigma_*) + \frac{1}{n}f(\sigma_*).$$

In terms of ε_* only,

$$w(\xi_*, p_{*n}^-) = +\frac{1}{2}\kappa\varepsilon_*^2 - \varepsilon_* y(1 + \frac{\kappa}{\alpha}) + \frac{1}{2\alpha}y^2(1 + \frac{\kappa}{\alpha}) + \frac{\kappa^2}{2n}\Big(\varepsilon_* - \frac{y}{\alpha}\Big)^2\Big(\frac{1}{\kappa} + \frac{1}{\alpha}\Big).$$

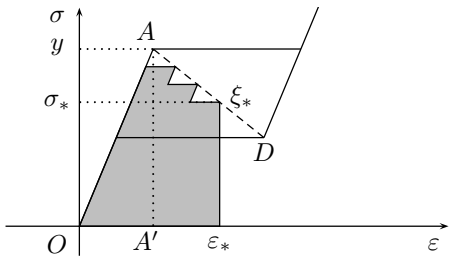

FIGURE 17. Work recovered to reach the origin starting from ξ_* ($n = 3$).

(iii) By paralleling the item (iii) of Lemma 4.1, we choose $p^-_{2n} = p^-_2 * p^-_n * p^-$, with duration $d^-_2 = d^+_2$, where p^- is given by (31), p^-_n is the sawtooth process obtained from (32) with a_n, b_n given by (25), and

$$p^-_2(t) = -1, \quad t \in [0, \varepsilon_2 - y/\alpha - h/\kappa).$$

In view of equations (6) and (10), we deduce $\varepsilon(d^+_2) = \sigma(d^+_2) = 0$ and the work recovered to reach the origin starting from ξ_2 is represented by the negative of the area of the grey-colored region in Fig. 18. Such area can be easily computed by adding the areas of the triangle OAA', the trapezoid $ADD'A'$ and the trapezoid beneath the segment $D\xi_2$ and then subtracting the area of the saw-shaped polygon above the segment AD:

$$\frac{1}{2\alpha}y^2 + \frac{h}{2\kappa}(2y - h) + \frac{1}{2}(\sigma_2 + y - h)\Big(\varepsilon_2 - \frac{y}{\alpha} - \frac{h}{\kappa}\Big) - \frac{1}{2n}h^2\Big(\frac{1}{\kappa} + \frac{1}{\alpha}\Big).$$

Some simple arrangements and the position (28) yield

$$w(\xi_2, p^-_{2n}) = -\frac{1}{2}\sigma_2\varepsilon_2 - \frac{1}{2\alpha}y(\alpha\varepsilon_2 - \sigma_2) + \frac{h(\alpha+\kappa)}{2\alpha\kappa}(\sigma_2 - y + h) + \frac{1}{n}f(y-h),$$

which proves the second part of this item. In terms of ε_2 only,

$$w(\xi_2, p^-_{2n}) = -\frac{1}{2}\alpha\,\varepsilon_2^2 + h\varepsilon_2(1 + \frac{\alpha}{\kappa}) - \frac{h}{2\alpha}(1 + \frac{\alpha}{\kappa})(2y + \frac{h}{k}) + \frac{1}{n}f(y-h).$$

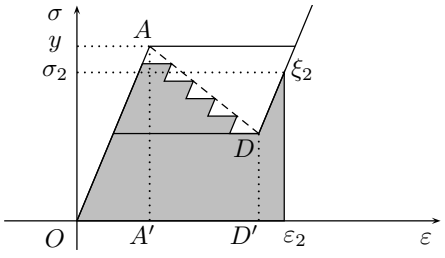

FIGURE 18. Work recovered to reach the origin starting from ξ_2 ($n = 5$).

(iv) By paralleling the item (iv) of Lemma 4.1, let $\xi_* = (\varepsilon_*, \sigma_*)$ be the point of the segment AD such that

$$\varepsilon_* = y/\alpha + (\alpha\bar{\varepsilon} - \bar{\sigma})/(\alpha + \kappa)\,, \tag{33}$$

$$\sigma_* = y - \kappa(\alpha\bar{\varepsilon} - \bar{\sigma})/(\alpha + \kappa)\,. \tag{34}$$

Then, we choose the process $\tilde{p}_n^- = \tilde{p} * p_n^- * p^-$, where p^- is given by (31), p_n^- is the sawtooth process obtained from (32) with a_n, b_n given by (24), and

$$\tilde{p}(t) = \begin{cases} +1 & t \in [0, \varepsilon_* - \bar{\varepsilon}), \quad \text{if } \bar{\xi} \in \Xi_1 \\ -1 & t \in [0, \bar{\varepsilon} - \varepsilon_*), \quad \text{if } \bar{\xi} \in \Xi_2, \end{cases}$$

so that $\rho(\bar{\xi}, \tilde{p}) = \xi_*$. The duration of $\tilde{p}_n^-$ is $\tilde{d}^- = \bar{d}^+$ and, in view of equations (6), (10), we deduce $\varepsilon(\tilde{d}^-) = \sigma(\tilde{d}^-) = 0$. Finally, from (12) and (27), we have

$$\begin{aligned} w(\bar{\xi}, \tilde{p}_n^-) \quad = \quad & -\int_0^{\bar{\varepsilon}-\varepsilon_*} \sigma(s)\, ds - \sum_{j=0}^{n-1} \int_{I_j^-} \left[y - \frac{n-j}{n}(y - \sigma_*) \right] ds \\ & + \sum_{j=0}^{n-1} \int_{I_j^+} \sigma(s)\, ds - \int_0^{y/\alpha} \sigma(s)\, ds. \end{aligned}$$

This value represents the negative of the area of the grey-colored region in Fig. 19. It can be easily computed by adding the areas of the triangle OAA' and the trapezoid beneath $A\xi_*$, then subtracting the area of the saw-shaped polygon above the same segment, and finally adding or subtracting (depending on the position of $\bar{\xi}$) the area of the trapezoid beneath the segment $\xi_*\bar{\xi}$:

$$\frac{1}{2\alpha} y^2 + \frac{1}{2}(y + \sigma_*)\Big(\varepsilon_* - \frac{y}{\alpha}\Big) - \frac{1}{2n}(y - \sigma_*)^2 \Big(\frac{1}{\kappa} + \frac{1}{\alpha}\Big) + \frac{1}{2}(\bar{\sigma} + \sigma_*)(\bar{\varepsilon} - \varepsilon_*).$$

By virtue of (33), (34) and the position

$$g(\bar{\xi}) = f(\sigma_*) = \frac{1}{2}\kappa^2 \left(\frac{1}{\kappa} + \frac{1}{\alpha}\right) \left(\frac{\alpha\bar{\varepsilon} - \bar{\sigma}}{\alpha + \kappa}\right)^2,$$

some simple arrangements yield

$$w(\bar{\xi}, \tilde{p}_n^-) = -\frac{1}{2}\bar{\sigma}\bar{\varepsilon} - \frac{1}{2\alpha} y(\alpha\bar{\varepsilon} - \bar{\sigma}) - \frac{\alpha\bar{\varepsilon} - \bar{\sigma}}{2(\alpha + \kappa)} \Big[y\Big(1 + \frac{\kappa}{\alpha}\Big) - \kappa\bar{\varepsilon} - \bar{\sigma} \Big] + \frac{1}{n} g(\bar{\xi}).$$

□

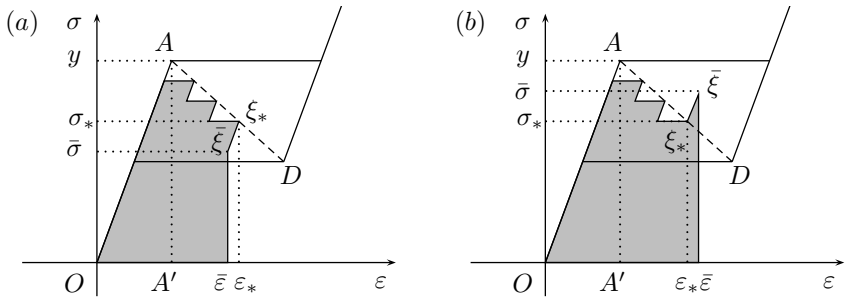

FIGURE 19. Work recovered to reach the origin starting from $\bar{\xi}$ ($n = 3$), when: (a) $\bar{\xi} \in \Xi_1$, (b) $\bar{\xi} \in \Xi_2$.

Acknowledgments. We are grateful to the referees for several valuable suggestions and comments.

REFERENCES

[1] F. Auricchio, *Considerations on the constitutive modeling of shape-memory alloys*, in "Shape Memory Alloys: Advances in Modelling and Applications" (eds. F. Auricchio, L. Faravelli, G. Magonette and V. Torra), CMINE: Barcelona, (2002), 125–187.

[2] A. Berti, C. Giorgi and E. Vuk, *Free energies in one-dimensional models of magnetic transitions with hysteresis*, Il Nuovo Cimento, B, **125** (2010), 371–394.

[3] V. Berti, M. Fabrizio and D. Grandi, *Phase transitions in shape memory alloys: A non-isothermal Ginzburg-Landau model*, Physica D, **239** (2010), 95–102.

[4] V. Berti, M. Fabrizio and D. Grandi, *Hysteresis and phase transitions for one-dimensional and three-dimensional models in shape memory alloys*, J. Math. Phys., **51** (2010), 062901.

[5] L. C. Brinson, *One-dimensional constitutive behavior of shape memory alloys: Thermomechanical derivation with non-constant material functions and redefined martensite internal variables*, Journal of Intelligent Material Systems and Structures, **4** (1993), 229–242.

[6] M. Fabrizio and A. Morro, "Electromagnetism of Continuous Media," Oxford University Press, Oxford, 2003.

[7] M. Fremond, *Materiaux a memoire de forme*, C. R. Acad. Sci. Paris Ser. II, **304** (1987), 239–244.

[8] M. Fremond, "Non-smooth Thermomechanics," Springer-Verlag, Berlin, 2002.

[9] V. I. Levitas and D. L. Preston, *Three-dimensional Landau theory for multivariant stress-induced martensitic phase transformations. I. Austenite↔martensite*, Physical Review B, **66** (2002), 134–206.

[10] S. Miyazaki, *Development and characterization of shape memory alloys*, in "CISM Courses and Lectures: Shape Memory Alloys," **351**. Springer: Wien, NewYork, (1996), 69–143.

[11] I. Müller, *Thermodynamics of ideal pseudoelasticity*, Journal de Physique IV, **C2-5** (1995), 423–431.

[12] I. Müller and S. Seelecke, *Thermodynamic aspects of shape memory alloys*, Math. Comp. Modelling, **34** (2001), 1307–1355.

[13] F. Nishimura, N. Watanabe, T. Watanabe and K. Tanaka, *Transformation conditions in an Fe-based shape memory alloy under tensile-torsional loads: Martensite start surface and austenite start/finish planes*, Material Science and Engineering, **A264** (1999), 232–244.

[14] C. M. Wayman, *Shape memory and related phenomena*, Progress in Materials Science, **36** (1992), 203–224.

[15] J. C. Willems, *Dissipative dynamical systems - Part I: General theory*, Arch. Rational Mech. Anal., **45** (1972), 321–351.

Received May 2011; revised October 2011.

E-mail address: alessia.berti@ing.unibs.it
E-mail address: claudio.giorgi@ing.unibs.it
E-mail address: elena.vuk@ing.unibs.it